

# PuzzleTuning: Explicitly Bridge Pathological and Natural Image with Puzzles

Tianyi Zhang<sup>1</sup> Shangqing Lyu<sup>2</sup> Yanli Lei<sup>1</sup> Sicheng Chen<sup>3</sup> Nan Ying<sup>1</sup>

Yufang He<sup>1</sup> Yu Zhao<sup>4</sup> Yunlu Feng<sup>5</sup> Guanglei Zhang<sup>1</sup>

<sup>1</sup>School of Biological Science and Medical Engineering,  
Beihang University, Beijing 100191, China

<sup>2</sup>Bioinformatics Institute (BII), Agency for Science, Technology and Research (A\*STAR),  
Singapore 138410, Singapore

<sup>3</sup>School of Microelectronics, Xi'an Jiaotong University, Xi'an 710049, China

<sup>4</sup>Department of Pathology, Peking Union Medical College Hospital, Beijing 100006, China

<sup>5</sup>Department of Gastroenterology, Peking Union Medical College Hospital, Beijing 100006, China  
{zhangtianyi, 20373207, 20101014, heiheyhe, guangleizhang}@buaa.edu.cn

lyusq@intern.bii.a-star.edu.sg 2201111586@stu.xjtu.edu.cn

yunluf@icloud.com rain986532@126.com

## Abstract

<https://github.com/sagizty/PuzzleTuning>.

*Pathological image analysis is a crucial field in computer vision. Due to the annotation scarcity in the pathological field, recently, most of the works have leveraged self-supervised learning (SSL) trained on unlabeled pathological images, hoping to mine the representation effectively. However, there are two core defects in SSL-based pathological pre-training: (1) they do not explicitly explore the essential focuses of the pathological field, and (2) they do not effectively bridge with and thus take advantage of the large natural image domain. To explicitly address them, we propose our large-scale PuzzleTuning framework, containing the following innovations. Firstly, we identify three task focuses that can effectively bridge pathological and natural domains: appearance consistency, spatial consistency, and misalignment understanding. Secondly, we devise a multiple puzzle restoring task to explicitly pre-train the model with these focuses. Thirdly, for the existing large domain gap between natural and pathological fields, we introduce an explicit prompt-tuning process to incrementally integrate the domain-specific knowledge with the natural knowledge. Additionally, a curriculum-learning training strategy is designed to regulate task difficulty, making the model adaptively fit the complex multiple puzzle restoring task. Experimental results show that our PuzzleTuning framework outperforms the previous SOTA methods in various downstream tasks on multiple datasets. The code, demo, and pre-trained weights are available at*

## 1. Introduction

Pathological image analysis is the gold standard in various medical diagnoses [23, 25]. Traditional pathological examination depends on the judgment of experts under the microscope, which is inefficient and may be affected by factors such as experience or fatigue [23, 25, 28]. In recent years, the advancement of deep learning (DL) has automated the diagnosis and has turned out to be a trend [8, 11, 25, 28].

The performance of DL-based pathological image analysis highly relies on the model initialization on large-scale datasets [8, 11, 25, 28]. The pre-training is therefore proposed regarding how to obtain the weight to initialize the models before finetuning them on specific downstream tasks. Significantly benefited from general vision knowledge, most researchers apply transfer learning [4, 8, 16, 23, 25–27], which initializes model weights from large-scale natural image pre-training. Still, the large domain gap between the natural and pathological image fields hinders the potential of such knowledge [4, 8, 16, 23, 25]. Therefore, rather than only transferring natural knowledge, some researchers focus on pathological image pre-training, where explicit modeling on pathological characteristics play a vital role [4, 16, 23, 25]. However, supervised pre-training relies on enormous training data, where labeled pathological images are of great scarcity. To address it, trending self-supervised learning (SSL) is used to pre-train models on large-scale unlabeled pathological images [4, 16, 18, 21–

[23, 25]. Taking advantage of general vision knowledge and mining effective feature representation with pathological focuses, expected SSL pre-training contributes to downstream performance and reliability. Correspondingly, two key challenges are identified for SSL pre-training in pathological image analysis: (1) The pre-training task should have explicit focuses on pathological characteristics. (2) The general vision knowledge should be effectively seamed with pathological knowledge to improve the generalization and robust abilities on downstream pathological tasks.

Regarding the first challenge, effective pre-training task objectives call for in-depth observations of pathological images and pinpointing their link to natural images. Specifically, due to pathological concepts such as intra-tumor heterogeneity [11], compared with natural images, the pathological image features present local similarities and global heterogeneity, and they are more discrete and are of multiple scales [4, 16, 21, 23, 25, 26]. The modeling process enhanced by permutations in [26, 27] inspires us to build relationship modeling tasks to bridge the natural general vision and pathological focuses. Additionally, inspired by the jigsaw puzzle task design of [20], the patch restoration concept suits our SSL ambition. To build an effective task with pathological focuses, we first identify three key relational focuses: appearance consistency, spatial consistency, and restoration understanding. Accordingly, Fig. 1 is illustrated by cropping and regrouping the patches of pancreatic liquid samples (a and b) and colonic epithelium tissue samples (c and d) of normal and cancer conditions.

**Appearance consistency.** Pathological images exhibit local homogeneity, where patches with similar concepts tend to cluster (e.g., within groups a, b, c, and d). However, when intermixing images from different organs (a+c, b+d) or within the same organ (a+b, c+d), the permuted relations disrupt this consistency, highlighting anomalies. The co-occurrence of patches of the same/different groups introduces grouping relationship on consistent/conflicting features [26, 27], which should be focused explicitly [23].

**Spatial consistency.** Adjacent patches in pathological images inherently share spatial relations. In Fig. 1, all patches numbered 4,7,8 (from groups a, b, c, and d) are fixed during shuffling. Their junction textures preserve spatial consistency in the same feature group. Among different groups, the junction patches present texture misalignment. Extrapolating such junction relationships can help models restore accurate tissue and cell cluster compositions [10, 13, 18, 24].

**Restoration understanding.** Opposite to understanding consistencies, correcting the misalignment scenarios offers another effective contrast learning goal [20, 23]. Specifically, learning the restoration among multiple swapped groups (1,3,5,9) vs. (4,7,8) explicitly focuses on the semantic alignment relationships. Additionally, pathological

images exhibit varied scales—ranging from individual cells (each patch in b), cell clusters (group of (b4,b7,b8) and (a4,a7,a8)), gland to tissue structures (c and d), necessitating a focus on multi-scale understanding [27].

However, current SSL pre-training task designs do not explicitly pinpoint these pathological focuses. Specifically, grouping the state-of-the-art (SOTA) SSL paradigm in computer vision (CV) [3, 7, 9, 10, 20–22, 24] as Contrastive Learning (CL) and Masked Image Modeling (MIM), their task designs encounter two barriers: First, MIMs reconstruct masked features through occlusion invariant learning on junction patches [10, 13, 21]. However, in addition to junction relationships in natural images, the pathological features demand explicit multi-scale modeling on grouping and semantic alignment relationships. Second, instead of spatial semantics, CL tasks mainly focus on grouping relationships based on general representation [3, 7, 9, 16]. Furthermore, the limited knowledge scope and category varieties of pathological images hinder the CL [16, 23].

Regarding the second challenge, the absence of explicit modules carrying the bridging knowledge hinders the performance of general vision knowledge. Firstly, pathological datasets are generally smaller and have a narrower knowledge scope than the diverse patterns in natural image datasets [4, 8, 25]. While transferring the general vision knowledge brings significant improvements [4, 16, 23, 25–27], the domain gaps set limitations on the downstream potential. Accordingly, previous pathology pre-training attempts [2, 18, 21–23] neglect general knowledge from natural images. While recently, domain-bridging learning has been proposed to take advantage of both methods [8]. However, most approaches finetune all parameters and move them from natural to pathological domain [21, 22, 25, 26]. Still, this implicit knowledge bridging overwrites the original general vision knowledge, which limits its generalization potential [8]. Advancing the pre-training calls explicitly integrating the domain-specific and general knowledge and effectively overcoming the gap between them [4, 8].

To address the challenges explicitly, we designed a novel SSL task to restore multiple puzzles for an enormous scale of unlabeled pathological images [25]. Effectively bridging natural and pathological domains, this SSL task explicitly focuses on the grouping, junction, and semantic alignment relationships at multiple scales. Specifically, a batch of input pathological images is broken into patches, and a fraction of these patches are shuffled among different images, tuning the batch into a state called ‘Puzzle’. Then, with a hint of the starting patches, the model is trained to restore the original image batch. Through the training, the model understands the grouping within multiple images, as well as the spatial junction relationships among the patches. By traversing multiple patch scales, the shuffling process introduces the multi-scale semantic alignment relationship.

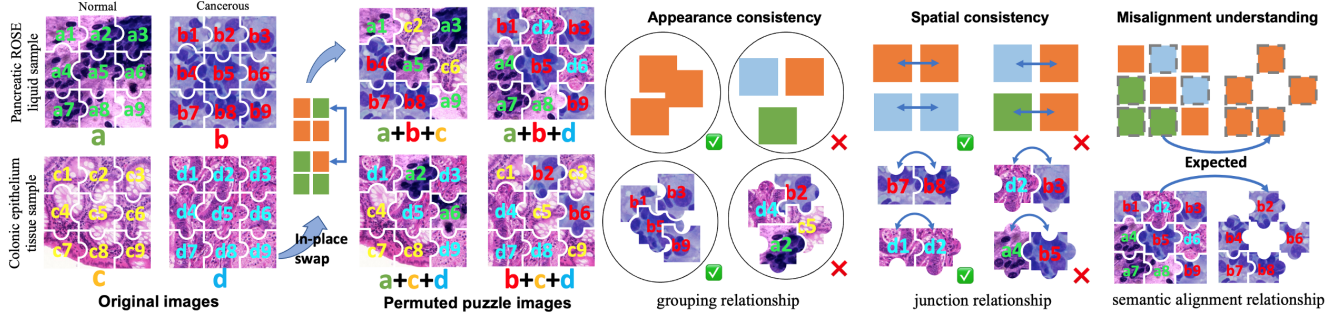


Figure 1. Samples illustrate the focuses and relationships in pathology. They are pancreatic liquid samples (a and b) and colonic epithelium tissue samples (c and d) of normal (a and c) and cancer conditions (b and d). The patches of them are numbered from 1 to 9.

Therefore, the puzzle pre-training task effectively bridges the domains with pathology and focuses on appearance consistency, spatial consistency, and restoration understanding.

Explicitly integrating pathological and natural general vision knowledge, we employ a prompting-based dataflow with additional prompt tokens [12]. We begin by initializing our model with weights pre-trained on natural images, encapsulating general vision knowledge. While fixing backbone parameters, we then update the prompt tokens using pathological images during training. Lastly, after pre-training, we finetune all parameters on downstream tasks. Additionally, we apply curriculum learning [1] to bridge the domain divergence between natural and pathological fields adeptly. This strategy emulates the human easy-to-hard learning trajectory, a method verified for its efficacy in complex tasks [1, 27]. Our practice is gauged by puzzle shuffling intricacy, starting with simpler mixing and increasing shuffling complexity over training. Covering multiple feature scales, we initiate pre-training with larger puzzle patches, narrowing down over epochs. This propagation in complexity and granularity bolsters the capacity for semantic understanding, adapting to the semantic gap of different images. With this strategy, our SSL pre-training approach is termed 'PuzzleTuning'.

In summary, our contributions are of four aspects:

1. Task focuses for pathology: By observing grouping, junction, and semantic alignment relationships at multiple scales, we identify three crucial task focuses in pathological pre-training: appearance consistency, spatial consistency, and restoration understanding. Based on them, we present a novel SSL pre-training task of multiple puzzles restoring, termed 'PuzzleTuning'.

2. Domain bridging with prompt-tuning: To effectively take advantage of general vision knowledge, we employ an explicit prompt-tuning technique. The prompt tokens, attached to the backbone, explicitly learn the bridging knowledge that seams the two domains.

3. Curriculum learning: We introduce an innovative

curriculum learning strategy that modulates the PuzzleTuning training difficulties, seamlessly adapting the multi-scale pathology focuses and general knowledge.

4. Large-scale SSL in pathology: Incorporating over 100 datasets of wide scope, this research is one of the most expansive SSL in pathological image analysis. Experimental results indicate that PuzzleTuning has surpassed previous SOTA methods in multiple downstream tasks.

## 2. Related Works

SSL pre-training can exploit large unannotated pathological image datasets. CL approaches are grounded in the premise that visually similar objects consistently possess identical labels. Widely applied CL representation learning frameworks, such as Virchow [22] based on DINO [2], TransPath [23] based on BYOL [7], MoCo [9], and SimCLR [3] based on Siamese architectures, have become staple frameworks in pathological image pre-training. Their training aims to learn representations that amplify alignment between analogous scenes while concurrently attenuating similarities among unrelated images [3, 7, 9].

Another SSL paradigm, MIM, is gaining prevalence over CL in pathological image analysis, attributed to its superior performance and training efficacy. The most representative MIM, Masked Auto Encoder (MAE) [10], randomly masks a large proportion of input images and reconstructs the obscured pixels through a lightweight decoder. By advancing occlusion invariant learning [13] in MAE, recent studies in pathological image analysis spotlight advancements. Specifically, GC-MAE [21] integrates local feature extraction of MAE with the global focus of contrast learning. SD-MAE [18] emphasizes the visible patches in MAE, utilizing a self-distillation mechanism to refine the junction modeling from pathological images. Extrapolating such junction relationship, the Siamese structured method SimMIM [24] is proposed to integrate the CL and MIM process.

Prompt tuning, proposed to align the knowledge gaps,

has become a prevalent method in pre-train models, which inspires researchers in the language and vision field [12, 15]. In prompt tuning, the parameters in the original pre-trained model are fixed, while only some additional parameters performing as prompt tokens can be updated through the pre-training. Severing as an incremental learning procedure [14, 15], the prompt tokens explicitly carry the extra information to align the downstream tasks. Therefore, explicit prompt-based structures can effectively encode additional domain-bridging knowledge during pre-training.

### 3. Methods

As illustrated in Fig. 2, three main processes are designed to explicitly bridge the domains with pathology focuses, including (1) Puzzle making process, (2) Puzzle understanding process, and (3) Puzzle restoring process.

#### 3.1. Puzzle Making Process

In the puzzle making process, we primarily introduce the shuffle strategy formulating the multiple puzzles, which explicitly train the model to mine the grouping, junction, and semantic alignment relationships with pathological images. Next, we traverse the patch sizes to explore the multi-scale relationship. From easy to hard with curriculum learning, we modulate puzzle mixing complexity.

##### 3.1.1 Multi-sample puzzle making

In puzzle making at Fig. 2, a batch of  $B$  pathological images ( $\tilde{I}_b$  with a size of  $3, h, w$ , where  $b = 1, \dots, B$ ), are broken into  $B$  bags. Each bag  $I_b$  is denoted as  $\{I_{1,b}, \dots, I_{m,b}\}$ , containing  $m$  patches, size of  $(3, P, P)$ . Next, under a fix-position ratio  $F_r$ , we assign some patches as fix-position patches  $I^{Pos}$ . They have the same randomly assigned position among all the  $B$  bags. In contrast, the remaining patches are assigned as relation patches  $I^{Rel}$ . This process generates

$$I_b = \{I_{1,b}^{Pos}, \dots, I_{r,b}^{Pos}, I_{r+1,b}^{Rel}, \dots, I_{m,b}^{Rel}\} \quad (1)$$

Then, the relation patches  $I^{Rel}$  from puzzle batch  $B$  are randomly swapped (in-place shuffled) among the bags, which changes the grouping relationship in new bags. Specifically, this in-place design makes the location index  $x \in \{1, \dots, m\}$  of each  $I_{x,b}^{Rel}$  unchanged while their batch indexes  $b \in \{1, \dots, B\}$  are re-assigned. The position patches  $I^{Pos}$  all stay unchanged in their original bags. They made up a puzzle state  $B_{puzzle} = \{\hat{I}_b, b \in [1, B]\}$  where each permuted bag  $\hat{I}_b$  is defined as

$$\hat{I}_b = \{I_{x_1,b}^{Pos}, I_{x_2,b'}^{Rel} | b' \in [1, B]; b' \neq b; x_1, x_2 \in [1, m]\} \quad (2)$$

After shuffling, for each pair of patches  $(I_{x_1,b}^{Pos/Rel}, I_{x_2,b}^{Pos/Rel})$  from the same original bag  $I_b$ , their absolute relationship remains unchanged, maintaining their original grouping relationship. In contrast, the grouping relationship in bag  $I_b$  is changed due to the pairs of  $(I_{x_1,b}^{Pos/Rel}, I_{x_2,b'}^{Pos/Rel})$ . Therefore, among permuted  $I^{Pos}$  and  $I^{Rel}$  patches from multiple bags, the design introduces new grouping and semantic alignment relationships. As shuffling creates new junction relationships of the patches, a series of puzzles presenting the three pathology focuses are ready to be learned.

##### 3.1.2 Curriculum design of puzzles

As shown in Fig. 3, with the curriculum learning concept, we build puzzles from easy to hard. During training, we gradually reduce the fix-position ratio  $F_r = f_e$  with a fix-position ratio scheduler on epoch  $e$ . Reducing  $f_e$  from 90% to 20%, the relationship complexity of permuted  $I^{Rel}$  is progressively increased [27].

Considering the multi-scale semantic alignment relationships, the granularity varies with the scale of pathological features. We traverse the patch size  $P = p_e$  by a patch-size scheduler on epoch  $e$ , which enables a more generalized and robust model with multiple feature scales of  $I_{x,b}^{Pos/Rel}$ .

#### 3.2. Puzzle Understanding Process

We explicitly seam the pathological focuses with general vision understandings in the puzzle understanding process. Firstly, the  $N_{Enc}$  layer encoder ViT [5] is built to model the identifications and relationships of the patches [26]. Then, based on VPT [12], we introduce additional prompt tokens into it, bridging the domains explicitly. Lastly, we design a special positional hint in the dataflow, which enables the proper restoration of shuffled puzzle bags.

##### 3.2.1 Encoder backbone

The ViT is applied to model the abstract relationships of the puzzle patches. For the ViT with  $N_{Enc}$  encoder layers  $L_n, n = 1, \dots, N_{Enc}$ ,  $k_{Enc}$  tokens of  $D_{Enc}$  dimension are learnt. Specifically, each puzzle  $\hat{I}_b$  of the input batch  $B_{puzzle}$  with position and relation patches  $I_{x,b}^{Pos/Rel}$  are embedded as position tokens  $T_{Pos}^0$  and relation tokens  $T_{Rel}^0$ .

Concatenated with an additional classification token  $T_{cls}^0$  and after the positional encoding process, the input for puzzle understanding becomes  $T_{Enc}^0 = [T_{cls}^0, T_{Pos}^0, T_{Rel}^0]$ . Then, the  $N_{Enc}$  layers of relationship encoding are formulated as

$$[T_{cls}^n, T_{Pos}^n, T_{Rel}^n] = L_n [T_{cls}^{n-1}, T_{Pos}^{n-1}, T_{Rel}^{n-1}] \quad (3)$$

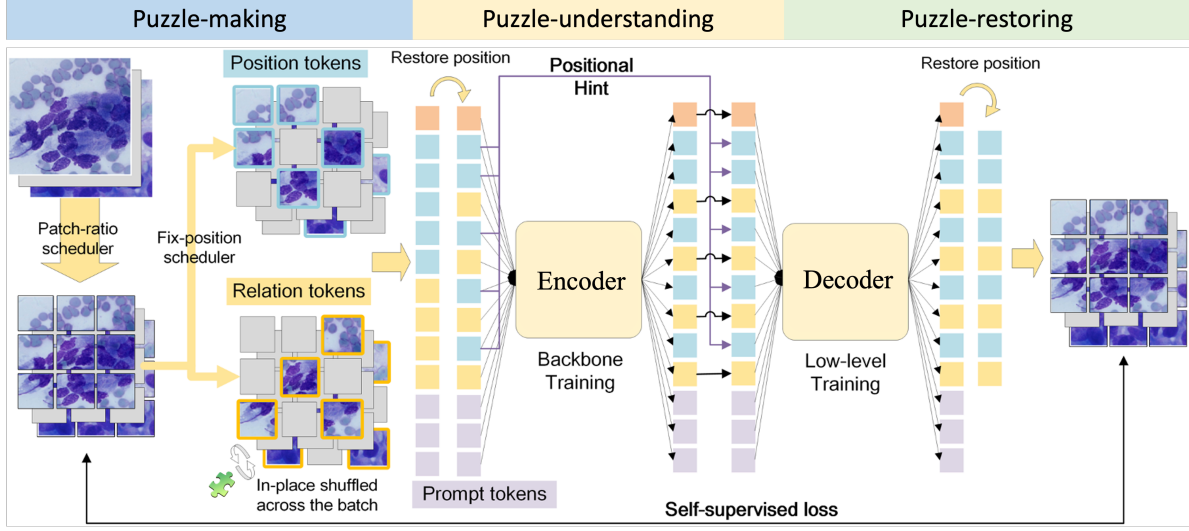


Figure 2. Three steps are designed in PuzzleTuning: 1) Puzzle making, where image batch are divided into bags of patches and fix-position and relation identity are randomly assigned. The relation patches are then in-place shuffled with each other, making up the puzzle state. 2) Puzzle understanding, where puzzles regarding grouping, junction, and restoration relationships are learned by prompt tokens attached to the encoder. Through the prompt tokens, the pathological focuses are explicitly seamed with general vision knowledge. 3) Puzzle reconstruction, where the decoder restores the relation tokens with position tokens as hint, under SSL supervision against original images.

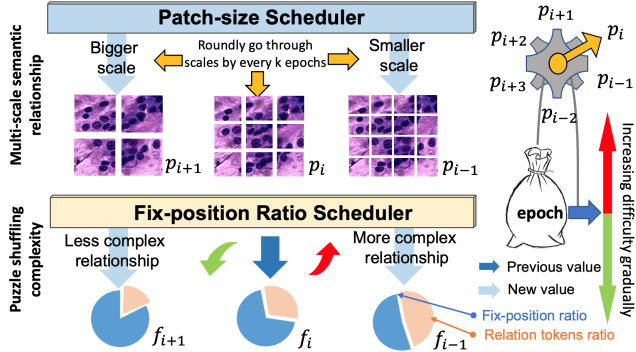


Figure 3. The curriculum learning design controls difficulty. During training, the difficulty gradually increases by decreasing the fix-position ratio. Additionally, the patch size roundly goes through all scales to capture the relationship at multiple scales.

After encoder modeling, all the output tokens  $[T_{cls}^{N_{Enc}}, T_{Pos}^{N_{Enc}}, T_{Rel}^{N_{Enc}}]$  of the last layer  $N_{Enc}$  will be used.

### 3.2.2 Prompt Tokens for domain bridging

Considering the general vision knowledge, we explicitly use prompt tokens to seam the pathological focuses into the pre-training process. As shown in Fig. 4, we build VPT-ViT encoders with additional prompt tokens at each encoder layer  $n$ . In the prompt training, only the prompt tokens  $P_n$  of VPT [12] will be updated to learn the pathological do-

main features. The remaining ViT parameters carrying the general vision knowledge are frozen. Following the VPT-Deep, the encoding is then formulated as follows.

$$[T_{cls}^n, T_{Pos}^n, T_{Rel}^n] = L_n[T_{cls}^{n-1}, T_{Pos}^{n-1}, T_{Rel}^{n-1}, P_n] \quad (4)$$

The encoder model patches relationships through puzzle understanding and the prompt tokens explicitly learn the domain-bridging knowledge aligning general vision.

### 3.2.3 Positional hint

As shown with purple lines in Fig. 2, the positional hint is a special design that enables the shuffled puzzle bags to be adequately restored. Specifically, after puzzle understanding, the original position tokens  $T_{Pos}^0$  replace the learned position tokens  $T_{Pos}^{N_{Enc}}$ . They serve as a hint of the puzzle starting point for upcoming puzzle restoring.

$$[T_{cls}^{N_{Enc}}, T_{Pos}^{N_{Enc}}, T_{Rel}^{N_{Enc}}] \rightarrow [T_{cls}^{N_{Enc}}, T_{Pos}^0, T_{Rel}^{N_{Enc}}] \quad (5)$$

Combined with the learned relation tokens  $T_{Rel}^{N_{Enc}}$  carrying the abstract information, each latent puzzle image  $\hat{I}_{latent}^b$  is obtained by restoring token locations. As the fix-position patches are randomly assigned, the positional hint is also flexible and only links the position tokens  $T_{Pos}^{N_{Enc}}$ . Following the same sequence of original input images  $I_{input}$ , the awareness of batch order for the decoder enables SSL loss supervision.

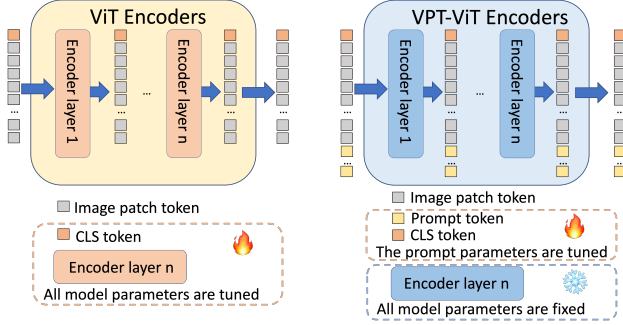


Figure 4. The prompting design of the encoder model. The additional prompt tokens employed explicitly seam the pathological focuses with the backbone’s general vision knowledge. Accordingly, only the prompt tokens will be tuned while the other model parameters are frozen.

$$[T_{Pos}^0, T_{Rel}^{N_{Enc}}] \rightarrow \{\hat{I}_{latent}^b \in \mathbb{R}^{3,h,w}\} \quad (6)$$

### 3.3. Puzzle Restoring Process

The decoder first embeds the latent puzzle image  $\hat{I}_{latent}^b$  into  $k_{Dec}$  tokens as  $T_{Dec}$ . Each token  $t_k^b$  is of the  $D_{Dec}$  dimension, where  $k = 1, \dots, k_{Dec}$ ,  $b = 1, \dots, B$ . Due to the decoder design, the feature dimension  $D_{Dec}$  can differ from the encoder dimension  $D_{Enc}$ .

$$T_{Dec} = \{t_k^b \in \mathbb{R}^{D_{Dec}}\} \quad (7)$$

Next, the decoder restores  $\hat{I}_{restore}^b$ , following the sequence of latent puzzle images  $\{\hat{I}_{latent}^b | b = 1, \dots, B\}$  with its corresponding hint  $T_{Pos}^0$  and learned latent tokens  $T_{Rel}^{N_{Enc}}$ .

$$\hat{I}_{restore}^b = \text{Decoder}(T_{Dec}) \quad (8)$$

Targeting to reconstruct the permuted relation patches  $I_{Rel}^b$ , we separate and resize the corresponding position tokens  $T_{Dec}^{Pos}$  and relation tokens  $T_{Dec}^{Rel}$ . Following their assignment at location index  $x$  and batch index  $b$ , the  $\hat{I}_{restore}^b$  is resized as

$$\hat{I}_{latent}^b = \{T_{Dec_{x_1,b}}^{Pos}, T_{Dec_{x_2,b}}^{Rel} | b \in [1, B]; x_1, x_2 \in [1, m]\} \quad (9)$$

The mean squared error (MSE) loss is applied for this SSL process, which supervises the decoder with the target patches  $I_{x,b}^{Rel}$  at location index  $x$  and batch index  $b$ .

$$\text{loss} = \text{MSE}(T_{Dec_{x,b}}^{Rel}, I_{x,b}^{Rel}) \quad (10)$$

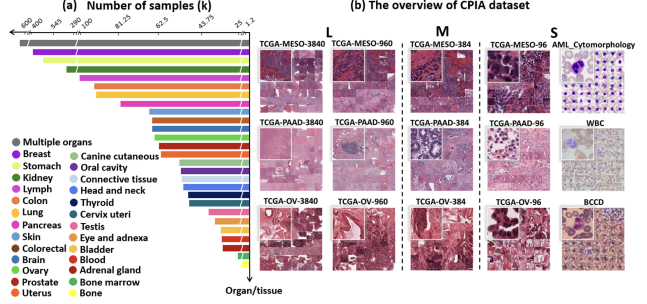


Figure 5. The data distribution and overview of the CPIA-Mini. (a) The organ/tissue categories and sample numbers of the CPIA-Mini dataset. Notably, the multiple organs category indicates that certain sub-datasets contain samples of more than one organ/tissue. (b) The thumbnail of the CPIA dataset. The CPIA-Mini dataset includes three scales reflecting the diagnosis habits of pathologists.

## 4. Experiment

In this section, we mainly explore and evaluate the effectiveness of PuzzleTuning.

### 4.1. Dataset and Implementation Details

#### 4.1.1 Dataset

Experiments in PuzzleTuning include two steps. The first is self-supervised pre-training, where a wide-covering CPIA dataset [25] is used. The second is fine-tuning, where four typical datasets representing different pathological feature scales are used.

In our pre-training stage, we utilized the CPIA-Mini dataset, a balanced subset of the comprehensive CPIA dataset, which amalgamates a variety of public datasets. CPIA-Mini consists of 3,383,970 images from 48 organs and tissues, covering 100 diseases. It is designed for broad coverage with efficient training. Notably, it includes three manually categorized sub-scales (L, M, and S) by expert pathologists to address the multi-scale nature of pathological image analysis. The data distribution and details of these sub-scales are presented in Fig. 5.

In finetuning stage, four diverse datasets are utilized to evaluate classification performance across multiple pathological scales from cellular to tissue level. These datasets are split in a manner reflective of their content: CAM16 [17], pRCC [6], and ROSE [26] are divided into training, validation, and test sets in a 7:1:2 ratio, while the WBC [19] dataset, considering its original separation, follows a 10:2:5 split. To ensure data integrity and prevent leakage, the ROSE and the test sets for other datasets are independent of CPIA-Mini. In addition to Tab. 1, more details of these datasets are provided as follows:

Camelyon16 (CAM16): From the Cancer Metastases in Lymph Nodes challenge, this dataset consists of 540 tu-

Dataset	Category Numbers	Image Numbers	Organ/Tissue	Feature Scale
CAM16	2	1081	Lymph Nodes	Tissue
pRCC	2	1417	Kidney	Glandular
ROSE	2	5088	Pancreas	Cellular
WBC	5	14514	Blood	Subcellular or Intracellular

Table 1. The overview of 4 fine-tuning datasets.

mors and 541 normal histopathology images, each cropped to 8000x8000 dimensions.

**Papillary Renal Cell Carcinoma Dataset (pRCC):** It includes 870 type I and 547 type II histopathology images, with an average size of 2000x2000. Type I images present small cells with clear cytoplasm, while Type II display cells with voluminous cytoplasm and high-grade nuclei.

**ROSE Dataset:** A private collection from Peking Union Medical College Hospital, this dataset contains cytopathology images from pancreatic liquid samples, including 1,773 pancreatic cancer and 3,315 normal images.

**Raabin-WBC Dataset (WBC):** Comprising cytopathology images of five blood cell types, it includes 301 basophil, 1,066 eosinophil, 3,461 lymphocyte, 795 monocyte, and 8,891 neutrophil images.

#### 4.1.2 Implementation Details

In PuzzleTuning pre-training, ViT-base is initialized with ImageNet, and then 20 prompt tokens are attached in each encoder layer. After 20 epochs of warm-up, 180 epochs are trained with a learning rate of 0.0001 and cosine weight decay to 0.05 times. The batch size is set to 256 images per GPU, and the puzzle group size is 16. The patch-scheduler controls puzzle patch sizes, altering scales looping from 16, 32, 48, 64, 96, and 112. The fix-position ratio scheduler linearly reduces the fixed-patch ratio from 90% to 20% to gradually increase the puzzle shuffling complexity.

After pre-training, on each downstream classification task, the pre-trained models are finetuned with multiple optimized hyper-parameters. For each output model, the average accuracy and F1-score on the top-5 best-performed experiments are reported. There are 4 A100 SMX4 GPUs used in pre-training and 4 RTX3090 GPUs used in downstream finetuning. More details of experiments are presented in the online release. Additionally, we present a Colab demo online for illustration at: <https://github.com/sagizty/PuzzleTuning>

## 4.2. Comparison with SOTA Methods

In this section, we benchmark several SSL SOTAs via equitable pre-training and finetuning. Following their release, the hyper-parameters of pre-training methods are optimized on CPIA [25]. The CL-based SSL methods such as Virchow [22] (DINO [2]) and TransPath [23] (BYOL [7]) in the pathological domain, and MoCo-V3 [9] and SimCLR

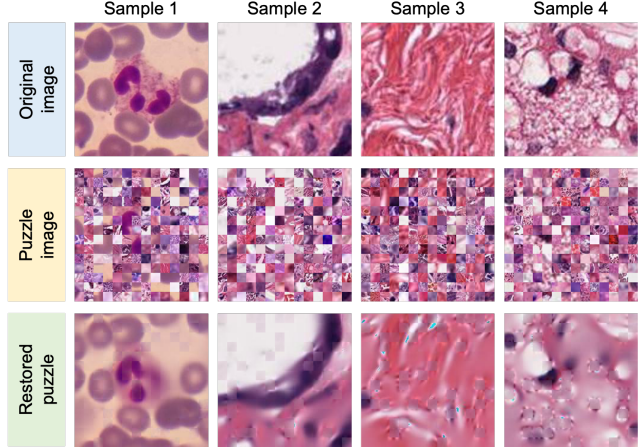


Figure 6. Samples and their permuted and restored puzzles, illustrating the SSL pre-training task of multiple puzzle restoring.

[3] in the general CV field are trained. We also evaluated recent MIMs such as MAE [10] and SimMIM [24] from the general CV field and their specialized counterparts for pathology, namely GC-MAE [21].

#### 4.2.1 Numerical performance

Equally to PuzzleTuning, these SOTA methods leverage the ImageNet pre-trained ViT-base and then are trained with the CPIA dataset. Their output models undergo finetuning with various hyper-parameters across four datasets, where the top-5 results are reported in Sec. 4.2. Results show that PuzzleTuning consistently outperforms these methods, achieving accuracy improvements of +3.89%, +6.92%, +6.89%, and +1.93% on CAM16, pRCC, ROSE, and WBC datasets. Generally, recent MIMs exhibit superior results to the CL methods. Among them, PuzzleTuning, through the explicit SSL pre-training task of multiple puzzle restoring, yields the highest performance. Achieving significant numerical improvements across all tasks, the explicit design bridges the general vision knowledge with pathological knowledge effectively, especially considering only prompt tokens are updated.

#### 4.2.2 Reconstruction performance

Regarding the explicit SSL task design of multiple puzzle restoration, with a batch of 4 images and their puzzles, Fig. 6 illustrates the reconstruction performance of PuzzleTuning. Specifically, regarding the appearance consistency, spatial consistency, and restoration understanding of Fig. 1, the reconstruction performance is visually demonstrated in Fig. 7 and Fig. 8.

In Fig. 7, guided by 25% of visible original patches to recover the entire image, both MAE and PuzzleTuning are

Method	CAM16			pRCC			ROSE			WBC		
	Acc(%)	F1-score	P-value	Acc(%)	F1-score	P-value	Acc(%)	F1-score	P-value	Acc(%)	F1-score	P-value
SimCLR	92.38	92.37	3.78E-18	92.30	91.66	2.93E-07	91.25	90.26	2.30E-10	97.73	96.26	1.01E-07
MOCO	83.12	82.94	3.34E-10	74.91	72.08	2.65E-21	72.02	63.57	6.95E-24	89.73	83.92	7.36E-12
TransPath (BYOL)	89.72	89.72	1.31E-09	73.52	70.76	8.38E-13	86.59	84.18	6.78E-03	94.81	91.50	6.83E-11
Virchow (DINO)	81.64	81.44	2.51E-17	73.05	69.59	6.04E-20	76.58	71.24	3.18E-10	88.88	82.48	4.24E-12
SimMIM	92.81	92.81	1.32E-12	87.99	86.96	3.46E-19	90.00	88.74	1.87E-12	96.76	94.74	1.29E-16
MAE	89.72	92.78	2.13E-13	93.10	92.70	2.32E-02	90.52	89.40	4.47E-10	97.69	95.98	4.94E-12
GCMAE	92.96	92.96	3.42E-14	90.15	89.36	1.15E-15	89.40	88.04	1.40E-13	96.79	94.79	4.25E-15
<b>PuzzleTuning</b>	<b>95.59</b>	<b>95.58</b>	-	<b>93.31</b>	<b>92.85</b>	-	<b>93.14</b>	<b>92.39</b>	-	<b>98.25</b>	<b>97.00</b>	-

Table 2. The average top-5 accuracy and F1-score comparison with SOTA pre-training methods on 4 downstream classification datasets including CAM16, pRCC, ROSE, WBC. P-values of paired-t test are given for comparison on F1-score, validating the PuzzleLearn’s performance.

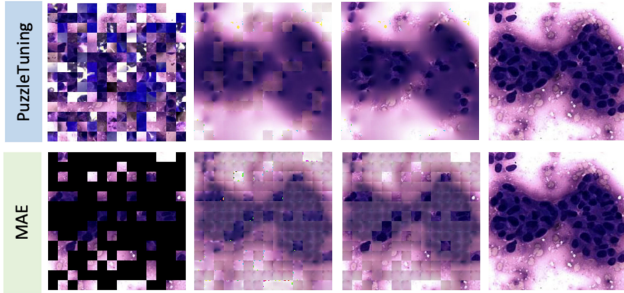


Figure 7. Illustrations of the permuted (masked or puzzled) samples and reconstructed images. The combined image has the visible patches (the unmasked patches or hint patches) replaced by the original patches, illustrating the consistency in MAE and PuzzleTuning.

trained with pathological understandings. However, the task focuses differ in their learning and restoring approaches, where PuzzleTuning employs multiple puzzles to explicitly learn the grouping, junction, and semantic alignment relationship. In contrast, MAE mainly focuses on interpreting the junction relationship of remaining patches with MIM. The extent of pathological image understanding can be reflected through restorations regarding two aspects: appearance consistency and spatial consistency.

Regarding appearance consistency, PuzzleTuning demonstrates a superior capability to reconstruct homogeneous global and local features compared to MAE. Globally, on the first image set of blood cells in Fig. 8, the combined image of PuzzleTuning closely resembles the original image with a low-saturation purple color feature, presenting a smooth and coherent appearance. In contrast, the MAE-generated patches display significant color differences from the original patches. Locally, PuzzleTuning consistently imparts the concave shape in the center of all surrounding red blood cells. In contrast, the MAE-generated images fail to preserve the concave shape of most red blood cells. Similarly, in Fig. 7, PuzzleTuning supplements cells based on limited visible original patches,

restoring cell clusters from the original image. However, MAE-generated images do not effectively restore cell morphology around visible patches, thus failing to achieve the desired consistency between cells.

Regarding spatial consistency presented with junction patches, PuzzleTuning excels in achieving smooth image reconstruction, preserving the advanced texture alignment toward visible original patches. On the contrary, the images generated by MAE exhibit relatively coarse connections between patches. Shown explicitly in the second set of Fig. 8 and Fig. 7, the edges between different patches in MAE-generated images become notably prominent. Their colors and textures present misalignment to the visible original patches. Additionally, the expected junction textures, such as rounded cell shape, which should be interpreted through the junction patches, are fuzzy in MAE-generated patches in Fig. 7. In contrast, PuzzleTuning reconstructs junction patches more clearly with continuous cell texture and color. Aligned closely with visible patches, PuzzleTuning clearly maintains spatial consistency through smooth transitions along patch edges.

## 5. Discussion

In this section, we mainly explore the proposed explicit designs in PuzzleTuning: domain-bridging, multiple puzzle restoration task, prompt tokens, and curriculum learning.

### 5.1. Domain-bridging Objective

Pathological image analysis has immensely benefited from general vision knowledge. However, the knowledge scope of the natural domain surpasses the pathological domain significantly. Therefore, PuzzleTuning seeks to merge the most effective knowledge aspects, and two critical focuses from natural images caught our interest: low-level semantic knowledge and high-level abstract vision.

In Tab. 3, the low-level semantic knowledge is obtained through occlusion-invariant learning by MAE [13]. Conversely, high-level abstract vision is obtained with traditional supervised classification training (timm). Using their

official ViT weights trained on ImageNet and contrasting them with random initialization, we finetune these ViT models to gauge their downstream effectiveness. We term these tests 'semantic', 'abstract', and 'random'. When employing PuzzleTuning pre-training on pathological images and subsequently finetuning the output models on specific tasks, we append these experiment names with '+PT'.

Initialization	CAM16		pRCC		ROSE		WBC	
	Acc	F1	Acc	F1	Acc	F1	Acc	F1
Random	80.93	80.67	70.39	65.65	71.71	62.88	90.28	84.09
Semantic	93.70	93.70	90.39	89.86	90.02	88.68	96.62	94.66
abstract	94.26	94.26	91.59	91.11	92.52	91.64	97.25	95.45
Random+PT	93.52	93.52	92.65	92.09	92.28	91.42	97.64	96.10
Semantic+PT	93.33	93.33	91.73	91.07	91.97	91.12	97.79	96.28
<b>abstract+PT</b>	<b>95.83</b>	<b>95.83</b>	<b>93.92</b>	<b>93.54</b>	<b>93.27</b>	<b>92.51</b>	<b>98.49</b>	<b>97.36</b>

Table 3. Average top-5 performance on 4 datasets, with different initializations (Random: randomly set weight of ViT; Semantic: MAE-trained ViT with ImageNet; abstract: supervised ImageNet-trained ViT), and +PT: means applying PuzzleTuning.

Firstly, we aimed to discern the type of knowledge initialization. As depicted in Tab. 3, across all four downstream classifications, the semantic knowledge group of occlusion-invariant learning via MAE generally underperforms the abstract vision group with supervised classification. Predictably, random initialization shows the worst performance due to the absence of any prior knowledge. Therefore, abstract initialization emerges as the most suitable general vision knowledge from the natural domain.

Next, the effectiveness of domain bridging is explored. In Tab. 3, all initialization exhibit significant improvements after PuzzleTuning. The results support the intention of explicitly bridging natural and pathological domains with pathological focuses. The multiple puzzle restoring task introduces focuses on multi-scale abstract grouping, and semantic alignment relationships, as well as low-level semantic knowledge of texture junction relationship. Furthermore, while the task in Tab. 3 is classification (which aligns more with abstract vision knowledge), the efficacy of applying semantic domain knowledge warrants further investigation.

## 5.2. Explicit Domain-bridging with Puzzles

Compared with the SSL MIM methods of MAE, GCMAE, and SimMIM in Sec. 4.2, PuzzleTuning achieves significantly higher performance in all downstream tasks. With its multiple puzzle restoring task, the additional abstract focuses of appearance consistency and restoration understanding are introduced. These explicit focuses improve the SSL on pathological samples in addition to occlusion-invariant learning of MIM [13], which only targets spatial consistency rooted in junction relationships.

To further explore this task, an ablation model of PuzzleTuning is specially designed by using the mask task from MAE. Their relation tokens are removed in the en-

coder (ViT), and the decoder is asked to predict the missing tokens. This ablation version is denoted as MAE, and the standard multiple puzzle restoring version is denoted as Shuffled Auto-Encoder (SAE) in Tab. 4. The numerical comparison underscores a general uptrend in the SAE over their MAE counterparts. Results suggest that, with explicit bridging focuses, the puzzle task is more effective than masking.

Tuning Methods	CAM16		pRCC		ROSE		WBC	
	Acc	F1	Acc	F1	Acc	F1	Acc	F1
<b>SAE-VPT+ft</b>	<b>95.83</b>	<b>95.83</b>	93.92	93.54	<b>93.27</b>	<b>92.51</b>	98.49	97.36
SAE-VPT+pt	94.17	94.17	90.74	90.08	92.01	91.09	<b>98.54</b>	<b>97.38</b>
SAE-ViT+ft	95.46	95.46	<b>95.19</b>	<b>94.84</b>	91.36	90.28	98.06	96.73
SAE-ViT+pt	92.13	92.12	82.26	80.41	87.40	85.93	97.34	95.58
MAE-VPT+ft	<b>94.35</b>	<b>94.35</b>	<b>91.10</b>	<b>90.36</b>	<b>89.98</b>	<b>88.84</b>	96.72	94.80
MAE-VPT+pt	91.02	91.01	87.28	85.96	89.86	88.53	<b>97.43</b>	<b>95.67</b>
MAE-ViT+ft	91.94	91.94	87.00	85.86	86.38	84.43	96.56	94.71
MAE-ViT+pt	91.02	91.02	82.33	80.89	85.77	83.72	96.67	94.42

Table 4. Average top-5 performance on 4 datasets, with different tuning methods (In pre-training: SAE: multiple puzzle restoring task proposed with PuzzleTuning, MAE: MAE method; ViT: ViT-base model, VPT: prompting with additional prompt tokens of ViT. In the downstream tasks: ft: finetuning all parameters, pt: prompting only the prompt tokens).

Reconstructions in Fig. 8 are visualized with the same 25% visible patches (the unmasked patches in MAE or hint tokens in PuzzleTuning). The images regenerated by PuzzleTuning bear a closer resemblance to their original appearances. The textures adjacent to the revealed patches are clearer, reflecting the junction relationships internalized by both methodologies. However, compared with SAE, MAE over-focuses on restoring the surrounding details of visible patches and struggles to effectively restore distant regions. Moreover, puzzle reconstructions display better color consistency regarding the original patch tokens, further validating its proficiency in assimilating the grouping relationship with its task focus of appearance consistency.

## 5.3. Explicit Domain-bridging with Prompt

Tab. 3 and previous sections underscore the efficacy of general vision knowledge, which provides a robust foundation for small dataset modeling. However, the differences between the pathological and general vision domains highlight misalignment in knowledge scope and sample variety. It calls for effective methods to combine domain-specific understanding and maintain generalized abilities for catering transfer learning to specialized tasks.

The utilization of prompt tokens stands out as an explicit strategy for conveying bridging knowledge while keeping the model backbone – representing general vision knowledge – unaltered. As delineated in Tab. 4, during pre-training, the SAE-VPT only turns the auxiliary prompt tokens, integrating puzzle understandings, whereas SAE-ViT finetunes the entire ViT backbone. As for the downstream

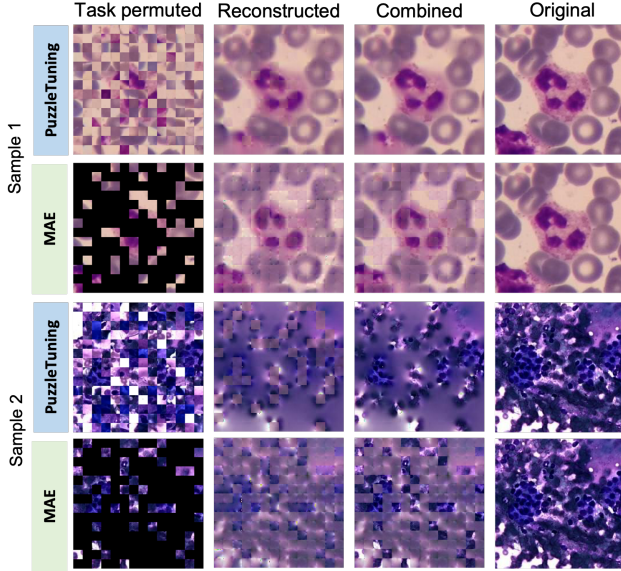


Figure 8. Illustrations of the permuted (masked or puzzled) samples and reconstructed images. The combined image has the visible patches (the unmasked patches or hint patches) replaced by the original patches, illustrating the MIM SSL task of MAE and PuzzleTuning.

phase, the 'pt' tag denotes only updating prompt tokens, and 'ft' represents updating the whole structure. Encountering the pre-trained ViT backbone, the downstream 'pt' combines the entire trained structure with empty additional prompt tokens. Conversely, if the pre-trained components are solely prompt tokens ('VPT'), the downstream model initializes the backbone ViT structure using timm weight and then attaches these pre-trained prompt tokens.

Tab. 4 suggests that the exclusive tuning of prompt tokens during pre-training tends to perform better ('VPT' groups surpass 'ViT' groups). This finding bolsters the strategy of seaming general vision knowledge with domain expertise. When trained on an extensive pathological dataset of CPIA, the additional prompt tokens explicitly assimilate bridging knowledge. Consequently, in downstream tasks, 'VPT' models endowed with this bridging knowledge achieve significant improvement.

Conversely, finetuning all parameters in downstream tasks generally achieves better performance ('ft' groups outshine the 'pt' groups). Due to the narrower knowledge scope and limited sample variety in specialized downstream datasets, finetuning the entire backbone allows for more precise calibration of both general and bridging knowledge. It ensures better fitting on small pathological datasets. Based on insights from both pre-training and downstream finetuning stages, the most efficacious setup emerges: adjust prompt tokens during pre-training and subsequently finetune both the backbone and prompt tokens in the down-

stream phase (VPT+ft).

## 5.4. Curriculum-based Domain-bridging

In pathological image analysis, multi-scale semantic knowledge is crucial. PuzzleTuning addresses this by varying puzzle patch sizes regulated by a patch-scheduler. Inspired by curriculum learning to improve the convergence, a fix-position ratio scheduler is designed, determining the proportion of un-shuffled patches. It modulates shuffling complexity and thus controls the task difficulty. In Tab. 5, this standard curriculum is denoted as 'base', which alternates patch sizes from 16 to 112 every three epochs while reducing the fix-position ratio from 90% to 20%.

Curriculum	CAM16		pRCC		ROSE		WBC	
	Acc	F1	Acc	F1	Acc	F1	Acc	F1
<b>base</b>	<b>95.59</b>	<b>95.58</b>	93.31	92.85	<b>93.14</b>	<b>92.39</b>	98.25	97.00
fixp16-ratiodecay	95.22	95.21	<b>93.92</b>	<b>93.48</b>	92.64	91.83	98.38	97.27
fixp16-fixr25	95.06	95.06	93.29	92.77	92.54	91.72	<b>98.45</b>	<b>97.27</b>

Table 5. Average top-5 performance on 4 datasets, with different PuzzleTuning curriculums. (base: patch size loop over the patches and fix-position ratio decay from 90% to 20%; fixp16-ratiodecay: patch size is fixed at 16 and fix-position ratio decays from 90% to 20%, fixp16-fixr25: patch size and fix-position ratio are fixed at 16, 25%).

Furthermore, additional curriculum ablations of 'fixp16-ratiodecay' and 'fixp16-fixr25' are designed with fixed patch sizes of 16 but differing fix-position ratios. All three curriculums surpass other SOTA methods significantly. Among them, the 'base' performs best in CAM16 and ROSE datasets, the 'fixp16-ratiodecay' excels in pRCC (+0.61% in accuracy), and the 'fixp16-fixr25' marginally (among 0.2% difference) leads in WBC. Overall, the dynamic patch approach in PuzzleTuning amplifies multi-scale understanding. Through aggregating complexity, the task difficulty gradually increases, and such curriculum learning further enriches the puzzle understanding.

## 6. Conclusion

In conclusion, PuzzleTuning is proposed as a potent SSL pre-training strategy tailored for pathological image analysis. Specifically, we devise an explicit multiple puzzle restoring task focusing on grouping, junctions, and semantic alignment relationships. Regulated by curriculum learning, the prompt tokens are leveraged to explicitly hone domain-bridging knowledge, seaming general vision with specific downstream pathological tasks. Pre-trained on a large-scale dataset and finetuned on multiple tasks, the significant improvements on various tasks prove its effectiveness and underscore the deliberate explicit design intentions.

## Acknowledgements

This work is partially supported by the National Natural Science Foundation of China, the Beijing Natural Science Foundation, and the Fundamental Research Funds for Central Universities.

Several collaborators have contributed to this work, specifically, we appreciate the early-stage support from our collaborator Chunhui Li from the School of Artificial Intelligence, Nanjing University. We appreciate the dedicated suggestions from Dr. Lee Hwee Kuan, Dr. Liu Wei, and Dr. Malay Singh as well as other members from the CVPD lab from Bioinformatics Institute (BII), Agency for Science, Technology and Research (A\*STAR), Singapore. We appreciate the project support from all team members at Beijing Advanced Innovation Center for Biomedical Engineering, School of Biological Science and Medical Engineering, Beihang University, China.

## References

- [1] Yoshua Bengio, Jérôme Louradour, Ronan Collobert, and Jason Weston. Curriculum learning. In *Proceedings of the 26th Annual International Conference on Machine Learning*, page 41–48, New York, NY, USA, 2009. Association for Computing Machinery. [3](#)
- [2] Mathilde Caron, Hugo Touvron, Ishan Misra, Hervé Jegou, Julien Mairal, Piotr Bojanowski, and Armand Joulin. Emerging properties in self-supervised vision transformers. In *2021 IEEE/CVF International Conference on Computer Vision (ICCV)*, pages 9630–9640, 2021. [2, 3, 7](#)
- [3] Ting Chen, Simon Kornblith, Mohammad Norouzi, and Geoffrey Hinton. A simple framework for contrastive learning of visual representations. In *Proceedings of the 37th International Conference on Machine Learning*. JMLR.org, 2020. [2, 3, 7](#)
- [4] Soham Rohit Chitnis, Sidong Liu, Tirtharaj Dash, Tanmay Tulsidas Verlekar, Antonio Di Ieva, Shlomo Berkovsky, Lovekesh Vig, and Ashwin Srinivasan. Domain-specific pre-training improves confidence in whole slide image classification, 2023. [1, 2](#)
- [5] Alexey Dosovitskiy, Lucas Beyer, Alexander Kolesnikov, Dirk Weissenborn, Xiaohua Zhai, Thomas Unterthiner, Mostafa Dehghani, Matthias Minderer, Georg Heigold, Sylvain Gelly, Jakob Uszkoreit, and Neil Houlsby. An image is worth 16x16 words: Transformers for image recognition at scale, 2021. [4](#)
- [6] Zeyu Gao, Bangyang Hong, Xianli Zhang, Yang Li, Chang Jia, Jialun Wu, Chunbao Wang, Deyu Meng, and Chen Li. Instance-based vision transformer for subtyping of papillary renal cell carcinoma in histopathological image. In *Medical Image Computing and Computer Assisted Intervention – MICCAI 2021: 24th International Conference, Strasbourg, France, September 27 – October 1, 2021, Proceedings, Part VIII*, page 299–308, Berlin, Heidelberg, 2021. Springer-Verlag. [6](#)
- [7] Jean-Bastien Grill, Florian Strub, Florent Altché, Corentin Tallec, Pierre H. Richemond, Elena Buchatskaya, Carl Doherty, Bernardo Avila Pires, Zhaohan Daniel Guo, Mohammad Gheshlaghi Azar, Bilal Piot, Koray Kavukcuoglu, Rémi Munos, and Michal Valko. Bootstrap your own latent a new approach to self-supervised learning. In *Proceedings of the 34th International Conference on Neural Information Processing Systems*, Red Hook, NY, USA, 2020. Curran Associates Inc. [2, 3, 7](#)
- [8] Hao Guan and Mingxia Liu. Domain adaptation for medical image analysis: A survey. *IEEE Transactions on Biomedical Engineering*, 69(3):1173–1185, 2022. [1, 2](#)
- [9] Kaiming He, Haoqi Fan, Yuxin Wu, Saining Xie, and Ross Girshick. Momentum contrast for unsupervised visual representation learning. In *2020 IEEE/CVF Conference on Computer Vision and Pattern Recognition (CVPR)*, pages 9726–9735, 2020. [2, 3, 7](#)
- [10] Kaiming He, Xinlei Chen, Saining Xie, Yanghao Li, Piotr Dollár, and Ross Girshick. Masked autoencoders are scalable vision learners. In *2022 IEEE/CVF Conference on Computer Vision and Pattern Recognition (CVPR)*, pages 15979–15988, 2022. [2, 3, 7](#)
- [11] Mariam Jamal-Hanjani, Gareth Wilson, Nicholas Mcgranahan, Nicolai Birkbak, Thomas Watkins, Selvaraju Veeriah, Seema Shafi, Diana Johnson, Richard Mitter, Rachel Rosenthal, Maximilian Salm, Stuart Horswell, Mickael Escudero, Nik Matthews, Andrew Rowan, Tim Chambers, David Moore, Samra Turajlic, Hang Xu, and Paulo De Sousa. Tracking the evolution of non-small-cell lung cancer. *New England Journal of Medicine*, 376, 2017. [1, 2](#)
- [12] Menglin Jia, Luming Tang, Bor-Chun Chen, Claire Cardie, Serge Belongie, Bharath Hariharan, and Ser-Nam Lim. Visual prompt tuning. In *Computer Vision – ECCV 2022*, pages 709–727, Cham, 2022. Springer Nature Switzerland. [3, 4, 5](#)
- [13] Xiangwen Kong and Xiangyu Zhang. Understanding masked image modeling via learning occlusion invariant feature. In *Proceedings of the IEEE/CVF Conference on Computer Vision and Pattern Recognition (CVPR)*, pages 6241–6251, 2023. [2, 3, 8, 9](#)
- [14] Brian Lester, Rami Al-Rfou, and Noah Constant. The power of scale for parameter-efficient prompt tuning, 2021. [4](#)
- [15] Xiang Lisa Li and Percy Liang. Prefix-tuning: Optimizing continuous prompts for generation, 2021. [4](#)
- [16] Tiancheng Lin, Zhimiao Yu, Zengchao Xu, Hongyu Hu, Yi Xu, and Chang-Wen Chen. Sgcl: Spatial guided contrastive learning on whole-slide pathological images. *Medical Image Analysis*, 89:102845, 2023. [1, 2](#)
- [17] Geert Litjens, Peter Bandi, Babak Ehteshami Bejnordi, Oscar Geessink, Maschenka Balkenhol, Peter Bult, Altuna Halilović, Meyke Hermesen, Rob Loo, Rob Vogels, Quirine Manson, Nikolas Stathonikos, Alexi Baidoshvili, Paul Diest, Carla Wauters, Marcory van Dijk, and Jeroen van der Laak. 1399 h&e-stained sentinel lymph node sections of breast cancer patients: The camelyon dataset. *GigaScience*, 7, 2018. [6](#)
- [18] Yang Luo, Zhineng Chen, Shengtian Zhou, and Xieping Gao. Self-distillation augmented masked autoencoders for histopathological image classification, 2023. [1, 2, 3](#)

- [19] Zahra Mousavi Kouzehkanan, Sepehr Saghari, Sajad Tavakoli, Peyman Rostami, Mohammadjavad Abaszadeh, Farzaneh Mirzadeh, Esmail Shahabi Satsar, Maryam Gheidishahran, Fatemeh Gorgi, Saeed Mohammadi, and Reshad Hosseini. A large dataset of white blood cells containing cell locations and types, along with segmented nuclei and cytoplasm. *Scientific Reports*, 12, 2022. [6](#)
- [20] Mehdi Noroozi and Paolo Favaro. Unsupervised learning of visual representations by solving jigsaw puzzles. In *Computer Vision – ECCV 2016*, pages 69–84, Cham, 2016. Springer International Publishing. [2](#)
- [21] Hao Quan, Xingyu Li, Weixing Chen, Qun Bai, Mingchen Zou, Ruijie Yang, Tingting Zheng, Ruiqun Qi, Xinghua Gao, and Xiaoyu Cui. Global contrast masked autoencoders are powerful pathological representation learners, 2022. [1](#), [2](#), [3](#), [7](#)
- [22] Eugene Vorontsov, Alican Bozkurt, Adam Casson, George Shaikovski, Michal Zelechowski, Siqi Liu, Philippe Mathieu, Alexander van Eck, Donghun Lee, Julian Viret, Eric Robert, Yi Kan Wang, Jeremy D. Kunz, Matthew C. H. Lee, Jan Bernhard, Ran A. Godrich, Gerard Oakley, Ewan Millar, Matthew Hanna, Juan Retamero, William A. Moye, Razik Yousfi, Christopher Kanan, David Klimstra, Brandon Rothrock, and Thomas J. Fuchs. Virchow: A million-slide digital pathology foundation model, 2023. [2](#), [3](#), [7](#)
- [23] Xiyue Wang, Sen Yang, Jun Zhang, Minghui Wang, Jing Zhang, Junzhou Huang, Wei Yang, and Xiao Han. Transpath: Transformer-based self-supervised learning for histopathological image classification. In *Medical Image Computing and Computer Assisted Intervention – MICCAI 2021*, pages 186–195, Cham, 2021. [1](#), [2](#), [3](#), [7](#)
- [24] Zhenda Xie, Zheng Zhang, Yue Cao, Yutong Lin, Jianmin Bao, Zhuliang Yao, Qi Dai, and Han Hu. Simmim: a simple framework for masked image modeling. In *2022 IEEE/CVF Conference on Computer Vision and Pattern Recognition (CVPR)*, pages 9643–9653, 2022. [2](#), [3](#), [7](#)
- [25] Nan Ying, Yanli Lei, Tianyi Zhang, Shangqing Lyu, Chunhui Li, Sicheng Chen, Zeyu Liu, Yu Zhao, and Guanglei Zhang. Cpia dataset: A comprehensive pathological image analysis dataset for self-supervised learning pre-training, 2023. [1](#), [2](#), [6](#), [7](#)
- [26] Tianyi Zhang, Youdan Feng, Yunlu Feng, Yu Zhao, Yanli Lei, Nan Ying, Zhiling Yan, Yufang He, and Guanglei Zhang. Shuffle instances-based vision transformer for pancreatic cancer rose image classification, 2022. [2](#), [4](#), [6](#)
- [27] Tianyi Zhang, Zhiling Yan, Chunhui Li, Nan Ying, Yanli Lei, Yunlu Feng, Yu Zhao, and Guanglei Zhang. Cellmix: A general instance relationship based method for data augmentation towards pathology image classification, 2023. [1](#), [2](#), [3](#), [4](#)
- [28] Zongwei Zhou, Vatsal Sodha, Md Mahfuzur Rahman Siddiquee, Ruibin Feng, Nima Tajbakhsh, Michael B. Gotway, and Jianming Liang. Models genesis: Generic autodidactic models for 3d medical image analysis. In *Medical Image Computing and Computer Assisted Intervention – MICCAI 2019*, pages 384–393, Cham, 2019. [1](#)